Spin probe dynamics of n-hexadecane in confined geometry

Miroslava Lukešová[1], Helena Švajdlenková[1], Pit Sippel[2], Eva Macová[1], Dušan Berek[1], Alois Loidl[2], and Josef Bartoš[1,a]

[1] Department of Structure and Physical properties, Polymer Institute of SAS, Dúbravská cesta 9, 84541 Bratislava, Slovakia
[2] Experimental Physics V, CEKM, University of Augsburg, 86135 Augsburg, Germany

Abstract. A combined study of the rotational dynamics of the stable free radical 2,2,6,6-tetramethyl-1-piperidinyloxy (TEMPO) and the phase behavior of n-hexadecane (n-HXD) in the bulk and the confined states in a series of silica gels (SG) by means of ESR and DSC is presented. A slow to fast motion transition of the spin probe TEMPO in the bulk n-HXD occurs at $T_{50\,\mathrm{G,bulk}} \ll T_{m,\mathrm{bulk}}$, i.e., well below the melting temperature due to its trapping and localized mobility in the interlamellar gap of the crystallites [J. Bartoš, H. Švajdlenková, M. Zaleski, M. Edelmann, M. Lukešová, Physica B **430**, 99 (2013)]. On the other hand, the dynamics of the TEMPO in the confined systems is strongly slowing down with $T_{50\,\mathrm{G}}(D_{\mathrm{pore}}) > T_m(D_{\mathrm{pore}})$ and slightly increases with the pore size $D_{\mathrm{pore}} = 60$, 100 and 300 Å of the SG's. At the same time, both the corresponding melting temperature, $T_m(D_{\mathrm{pore}})$, and melting enthalpy, $\Delta H_m(D_{\mathrm{pore}})$, decrease with D_{pore} together with the mutual anti-correlation between $T_{50\,\mathrm{G}}$ and T_m as a function of the inverse of pore diameter, $1/D_{\mathrm{pore}}$. Moreover, the dynamic heterogeneity of the TEMPO in the confined state below $T_{50\,\mathrm{G}}(D_{\mathrm{pore}})$ is closely related to the phase transformation. The strong slowing down of the spin probe motion likely results from its preferential localization at the interface layer of the matrix pore due to specific interaction of TEMPO molecules with the polar silanol groups of the SG matrix. This is supported by special study on a series of the variously filled n-HXD/SG systems, other similar experimental findings as well as by theoretical spectral argument.

1 Introduction

From thermodynamic, structural and dynamic studies of a variety of organic compounds in the bulk and the confined state by internal probes of macro- and microscopic techniques [1–6], it is well-known that their confinement in porous matrices can lead to essential changes in their physical structure and related physical properties [7–27]. Thermodynamic behavior of crystallizing organic media in porous confiners as monitored by differential scanning calorimetry (DSC) exhibits either mostly negative or sometimes positive shift of the phase transition temperatures as well as reduction of the corresponding phase transformation enthalpies as a function of pore size with respect to the bulk state [7–13]. These trends in the former quantities are often interpreted in terms of the Gibbs-Thompson equation [14], although this type of classic thermodynamic treatment of confinement phenomena breaks down for very small pores due to finite size and inhomogeneity effects. Structural studies of some crystallizing confined systems using X-ray diffraction and solid-state NMR also indicate significant morphological reorganization through the phase separation, and sometimes, with the formation of new type of ordered phase of filler [15–19]. Finally, dynamic studies performed on a variety of the

[a] e-mail: Jozef.Bartos@savba.sk

confined organics by NMR [18,19] and dynamic investigations by DS and BDS [10,20–23] and NS [24–27] revealed the sensitivity of relaxation to the geometry parameters of confining matrix as well as to the surface physical chemistry, i.e., solvophobicity or solvophilicity effect of the medium. In some cases, formation of a new phase within filler has been attributed to the contact layer (interface) of the confined material at the pore wall [7–13,20–23]. At present, it is widely accepted that the confining effect on structural and physical properties as obtained from traditional internal probing techniques results from a complex interplay of the spatial limitation of medium in the porous matrix (finite size factor) and the mutual interaction between the constituents of filler and confiner (interfacial factor) in the confined systems [1–6].

On the other hand, although the characterization of confined media by special microscopic techniques utilizing external probes appeared at the very beginning of systematic studies of the confinement problem [28,29], such types of investigations are essentially less common. This is despite the fact that they provide very valuable information about the physical factors controlling the dynamic and transport behavior of some small particles under geometric restriction with potential impact on various important fields of nanoscience and nano-technology such as physical separation, chemical reactivity and catalysis

in nanoreactors, etc. Among them, besides positron annihilation lifetime spectroscopy (PALS) using atomic-sized ortho-positronium (o-Ps) probe which measures simultaneously free volume in both the medium and matrix components of the confined system [30–32], molecularly-sized ones such as spin probes based on stable nitroxide free radicals using electron spin resonance (ESR) are of a great importance. The stability of aliphatic nitroxides, the relative simplicity of their ESR spectra, and, in particular, the sensitivity of ESR spectra to environmental changes make them to objects of considerable interest and wide application in solving the specific microstructure and microdynamic problems such as the metastable supercooled water, functionalized porous polymers [33–38]. In contrary to PALS, ESR detects the confined medium only being insensitive to the inner parts of the confiner. Several ESR investigations on the dynamic behavior of various spin probe nitroxides dissolved in various inorganic and organic media embedded in different porous matrices were reported [39–42]. So far, these ESR studies were concentrated on simple molecular media, especially water and several common organic solvents such as simple aliphatic alcohols, aliphatic and aromatic cyclic hydrocarbons in irregular matrices such as silica gels and Vycor [39–41,43–45] as well as some regular ones such as zeolites and MCM-41 [46–54]. Two main findings were reported [43–54]: (i) independent of the spin probe nature, its mobility was lower after confinement and (ii) in some cases, especially for the very highly confined samples in SG with $D_{\text{pore}} \sim 40$ Å and in still smaller pores of zeolites and positively charged spin probes, superimposed ESR spectra were observed and the co-existence of different moving stable radicals was attributed to the inhomogeneous character of the complex three component confined systems. The specific aspect of ESR studies of confined systems, i.e., potential interaction of the molecular probe particle with the surface wall of the matrix pores was also addressed using various structural types of nitroxides. It was argued that whereas the positively charged spin probes strongly interact with the surface of SG and MCM-41 matrices, both the neutral and negatively charged ones are not strongly influenced under spatial restriction, so that they correctly reflect the structural-dynamic state of the confined medium [43–48]. In contrast to low-molecular media, internal probe studies on the confined oligomeric n-alkanes systems are rather sporadic. While some thermodynamic, structural and dynamic data on some shorter liquid alkanes in CPG's and SG's by DSC [7,12,13], shorter n-hexane and longer n-eicosane and n-heneicosane in MCM-41 by NMR [18,19], n-hexane in SG's or silicon by NS [26,27] were reported, those on liquid n-alkanes of intermediate lengths are scarce [16,17]. As for external probes, according to our best knowledge, ESR studies on this type of organic compounds are almost absent. Moreover, since most of the afore-mentioned fillers are crystallizing media in the bulk state, they can undergo phase transformations under spatial restriction, this combining aspect of the complex mutual acting of spin probe dynamics and phase behavior has not been simultaneously addressed in detail.

Recently [55], we investigated the rotational dynamics of one of the smallest neutral nitroxide spin probes TEMPO in both the solid and liquid bulk states of the typical intermediate chain organic compound n-hexadecane (n-HXD) over a wide temperature range by ESR, DSC as well as PALS techniques. It was found that the most pronounced characteristic ESR temperature of the slow to fast transition, $T_{50\,\text{G}}$, for the spin probe TEMPO [56] lies significantly (about 100 K) below the melting point of n-HXD and this finding was ascribed to the trapping of the TEMPO molecules in an interlamellar gap of the crystalline lamellae of n-HXD and to the molecular deformation induced enhanced mobility of the ends segments of the linear alkane chains [55].

This contribution presents a systematic combined external and internal probe study on n-hexadecane (n-HXD) in several irregular inorganic matrices. The dynamics of the spin probe TEMPO in the bulk crystalline n-HXD and that of very diluted n-HXD/TEMPO solution inserted into three silica gels (SG) of different pore sizes revealed by ESR technique is related to the thermodynamic phase behavior of n-HXD in both the bulk and the confined states as detected by DSC. The aim is to assess the role of spatial restriction in the mutual relationship of small molecule dynamics and phase change of the medium employed with emphasis on the specific aspect of external probing, i.e., additional modes of interaction between the molecular probe and the medium and/or the surface wall of the matrix. Subsequently, the ultimate goal of our systematic studies is to find out the limits of external spin probe ESR technique for characterization of various types of confined organic compounds via observed changes in the dynamics of small molecule in the corresponding filler – confiner system.

2 Experimental

2.1 Materials

n-Hexadecane (n-HXD) from Sigma-Aldrich, Inc, Germany with 99% purity was used as a medium confined in a series of three silica gels (SG), Kromasil® from Eka Chemicals AB, Separation Products, Sweden with a mean spherical particle size of 10 μm characterized by a complex network of roughly cylindrical pores. The basic physical parameters of these matrices from supplier determined by BET and N_2-adsorption methods are listed in Table 1.

As the external probe, 2,2,6,6-tetramethylpiperidine-1-oxyl, (TEMPO), from the same company as n-HXD, was applied by simply dissolving in the liquid n-HXD at concentration of about 4×10^{-4} spin/mol.

A series of the confined spin systems for ESR studies was prepared step by step (drop by drop) filling of n-HXD that contained the probe into the accessible pores of SG matrices to achieve the completely filled (saturated) state of the filler (n-HXD) in the pores of the confiner (SG) expressed as the mass fraction of the filler (n-HXD) to the total mass of the filler + matrix (n-HXD + SG) system.

Table 1. Physical parameters of a series of the used SG matrices.

Matrix	Pore diameter D_{pore}, Å	Pore volume V_{pore}, cm^3/g	Pore area S_{pore}, m^2/g	$F^*_{\text{HXD,theo}}$ –	$F^{**}_{\text{HXD,sat}}$ –	%
SG 60	60	1.20	540	0.480	0.227	47.3
SG 100	100	0.85	309	0.395	0.325	82.3
SG 300	300	0.93	105	0.417	0.302	72.4

*$F_{\text{HXD,theo}} = m_{\text{HXD}}/(m_{\text{HXD}} + m_{\text{SG}})$, theoretical mass fraction of n-HXD medium with respect to the n-HXD/SG system calculated using the density of n-HXD at room temperature, ρ_{HXD} (RT) = 0.77 g/cm^3 under the complete accessibility condition of all pores for the n-HXD medium. **$F_{\text{HXD,sat}} = m_{\text{HXD}}/(m_{\text{HXD}}+m_{\text{SG}})$, experimental mass fraction of n-HXD in the n-HXD/SG system corresponding to the completely filled (saturated) situation of the n-HXD in the n-HXD/SG system.

The capillary forces allowed to fill the pores of silica gel with n-HXD and its solution to different extent including the situation when actually no liquid remained on the silica gel surface. This was also confirmed by means of low-T DSC by the appearance of the single melting peak, indicating the pore melting of the medium localized inside the accessible pores only and on the absence of the so-called "bulk" melting endotherm of the medium situated outside the matrix grains [7–13] – in detail see below. To test the fullness factor of the spin probe and closely related localization aspect of the problem, a series of the n-HXD/SG 100 Å systems with various degree of filling was prepared. Before the own filling procedure the SG matrices were dried at 120 °C for elimination of traces of adsorbed water. The confined samples for DSC measurement were obtained by the same procedure using pure n-HXD as a filler. The external probe TEMPO may, in principle, act as a nucleation admixture (agent) causing an accelerated onset of the crystallization transformation. Our control tests on this possible effect of the very dilute TEMPO solution on the freezing in both the bulk and the confined systems showed no change within experimental uncertainty ±0.5 K in the characteristic DSC temperatures. This is in consistency with a very small amount of the probe additive in the doped bulk and confined samples.

2.2 Techniques

ESR

ESR measurements of spin probed n-HXD were performed on a the X-band Bruker – ER 200 SRL operating at 9.4 GHz with a Bruker BVT 100 temperature controller unit. ESR spectra of the doped n-HXD/TEMPO systems cooled with about –5 K/min were recorded during subsequent heating over a wide temperature range from 100 K up to 360 K with steps of 5–10 K. The sample was kept at the given temperature at thermal equilibrium before the spectra were accumulated. The temperature stability was ±0.5 K. The microwave power and the field modulation amplitude were optimized to avoid signal distortion. Evaluation of the ESR spectra was performed in terms of the spectral parameter of mobility, $2A_{zz'}$, as a function of temperature with pore size, D_{pore}, as a system parameter with the subsequent evaluation of spectral parameter of

mobility $T_{50\,\text{G}}$ parameter [56] and some further characteristic ESR temperatures in both the slow and fast motion regimes [55–59].

DSC

DSC measurements were carried out on DSC 8500 Pyris from Perkin Elmer based on power compensation principle equipped with a CLN2 Cooler. Calibration was performed with a series of three different standard substances: indium, n-dodecane and n-heptane. The sample masses were about 15 mg. All DSC measurements were carried out under nitrogen atmosphere using standard aluminium pans. The samples were cooled with –5 K/min from room temperature down to 173 K and subsequently were measured with heating rate of +10 K/min from 173 K up to 333 K. The melting phenomenon, i.e., endothermal effects in the DSC thermogram, were quantified by the onset melting temperature, $T_{m,\text{on}}(D_{\text{pore}})$, from now marked as $T_m(D_{\text{pore}})$, and the corresponding melting enthalpy, $\Delta H_m(D_{\text{pore}})$, normalized to the mass of n-HXD.

3 Results

3.1 DSC responses and the phase transition parameters

Macroscopic characterization of bulk n-HXD and confined n-HXD/SG was performed via monitoring their thermodynamic phase behavior by DSC. Two types of DSC studies were carried out: (1) the first one served for checking the applied filling procedure and further special particular studies of effects of the degree of repletion and (2) the second for the quantitative thermodynamic characterization of a series of completely filled n-HXD/SG systems.

In the first type of DSC measurements the filling procedure of the SG's pores was controlled by measuring the DSC traces as function of the relative degree of filling of the given matrix by the medium, F_{HXD}, for the individual pore sizes, D_{pore}. Figure 1 displays a series of the DSC thermograms with the various n-HXD fraction for the n-HXD/SG 100 Å system as a representative example. Figure 2 shows both the thermodynamic parameters of the melting process (T_m, ΔH_m) as a function of the fraction of n-HXD medium in the n-HXD/SG systems. A qualitative change in the evolution of DSC scans with
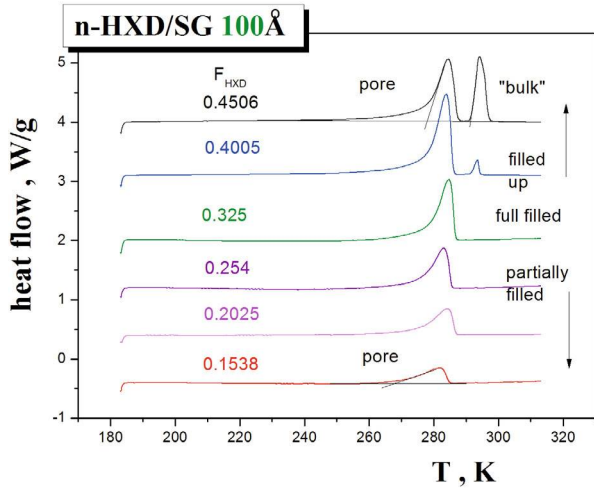
Fig. 1. DSC scans of a series of the n-HXD/SG 100 Å samples with the various degrees of filling of SG matrix by n-HXD, F_{HXD}, in the overfilled states with $F_{HXD} = 0.4506$ (black) and 0.4005 (blue), in the fully filled state $F_{HXD,sat} = 0.325$ (green), and in the partially filled states with $F_{HXD} = 0.2540$ (violet), 0.2025 (magenta) and 0.1538 (red). DSC thermograms are shifted for clarity.

increasing n-HXD fraction from one peak endotherm response at lower filling levels to that with the two peak endotherm effect at the highest filling one is evident. The presence of one or two endotherm effects in the DSC thermograms indicates the existence of one or two kinds of the n-HXD medium in the n-HXD/SG 100 Å systems, respectively. From Figure 2 it follows that the first endotherm characterized by the lower T_m values is to some extent sensitive to the F_{HXD} in contrast to the other one, which has the same onset melting temperature as the bulk n-HXD sample $T_{m,bulk} = 291.4$ K (see below). Thus, the latter effect can be attributed to the melting of a part of the n-HXD material localized outside of the grains of the SG 100 Å matrix which can be marked as "bulk" n-HXD. This corresponds to the overfilled situation of the two n-HXD/SG samples. On the other hand, the former endotherms with the lower T_m's, being dependent on the fraction of n-HXD, are ascribed to the phase transformation of a part of the n-HXD medium embedded inside of the pores of the SG 100 Å matrix in the partially filled state. Finally, the last DSC trace of this series with $F_{HXD,sat} = 0.325$ exhibiting single endotherm, corresponds just to the saturated situation, named the full filled (saturated) sample.

The other type of DSC studies addresses the actual confinement effect on thermal behavior in the n-HXD/SG systems. Figure 3 displays a series of DSC scans for n-HXD in the bulk state as well as for a series of the three confined states of n-HXD/SG system in dependence on the mean pore diameter, D_{pore}, at the corresponding n-HXD fractions, $F_{HXD,sat}$, from Table 1.

Figure 4 shows the onset melting temperature, T_m, and melting enthalpy, ΔH_m, parameters of the melting process as a function of the mean pore size, D_{pore}, of the three completely filled SG matrices together with one additional
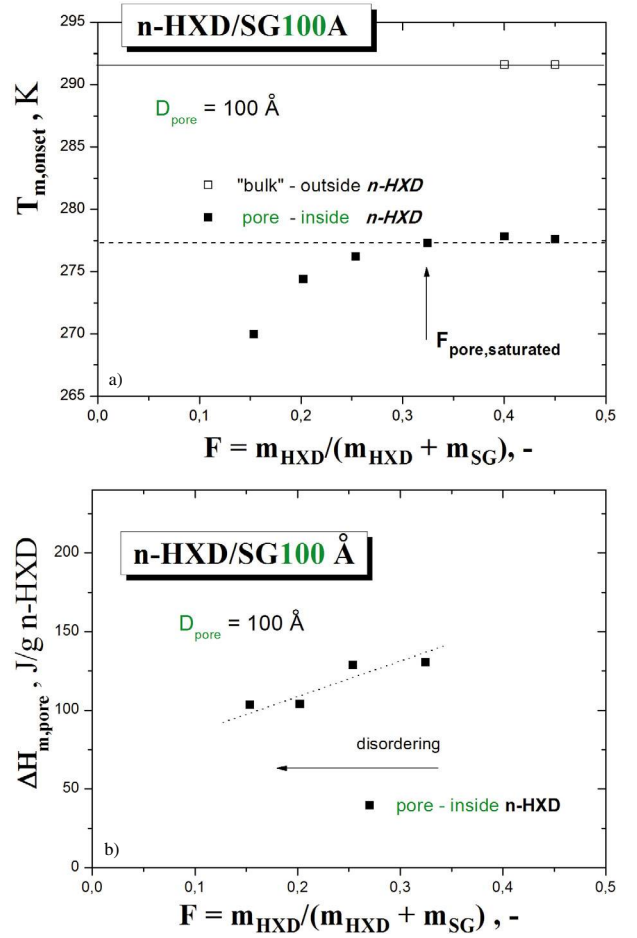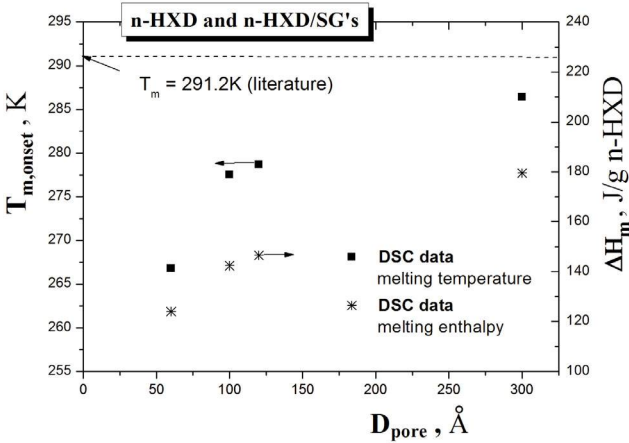

Fig. 2. (a) Onset melting temperature, T_m, and (b) melting enthalpy, ΔH_m, as a function of the fraction of n-HXD in the n-HXD/SG 100 Å system. In (a) the upper horizontal line marks the onset melting temperature of the bulk n-HXD sample, $T_{m,bulk} = 291.4$ K, in agreement with the literature [60,61].
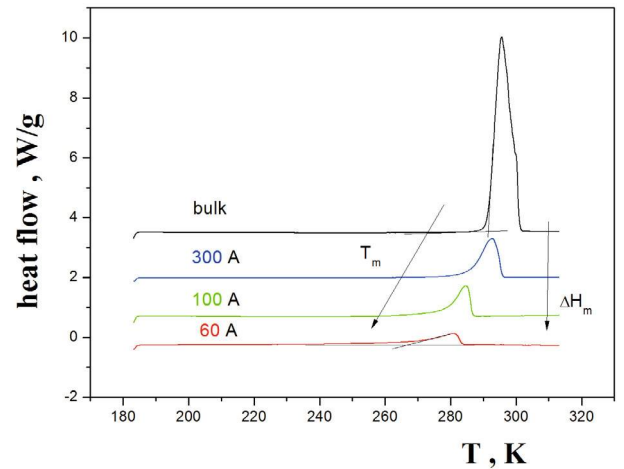
Fig. 3. DSC scans of the bulk n-HXD sample (black) with $D_{pore} = \infty$ and a series of the n-HXD/SG systems with $D_{pore} = 300$ Å (blue), 100 Å (green) and 60 Å (red) at the corresponding saturated fractions of n-HXD, $F_{HXD,sat}$ (see Tab. 1). DSC thermograms are shifted for clarity.
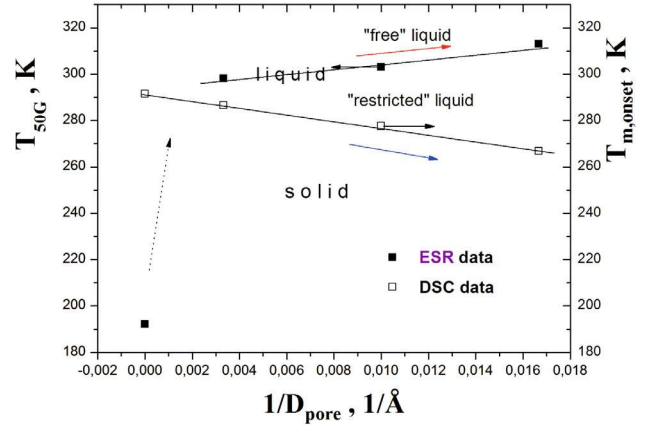
Fig. 4. Onset melting temperature, T_m, and melting enthalpy, ΔH_m, of the saturated n-HXD fraction in the n-HXD/SG systems in dependence on the mean pore diameter: $D_{\text{pore}} = 60$, 100 and 300 Å of the used SG matrices. The T_m and ΔH_m values for one additional SG matrix with $D_{\text{pore}} = 120$ Å are also included. The upper horizontal line indicates the melting temperature of bulk n-HXD, $T_{m,\text{bulk}} = 291.4$ K.


Fig. 5. Test of the Gibbs-Thompson equation for the melting temperature in terms of $T_m(D_{\text{pore}})$ vs. $1/D_{\text{pore}}$ (right scale) together with the $T_{50\,G}$ vs. $1/D_{\text{pore}}$ dependence (left scale). In the former case the thick line corresponds to a linear fit of the $T_m(D_{\text{pore}})$ values for the four confined n-HXD/SG systems, by extrapolation giving an intercept $T_m(D_{\text{pore}}) = (291.4 + / - 0.75)$ K for $D_{\text{pore}} \to \infty$ close to the literature value $T_{m,\text{bulk}} = 291.2$ K [60,61].

result for $D_{\text{pore}} = 120$ Å. The former quantity decreases with decreasing pore size from $T_m(\text{bulk}) = 292.4$ K for the bulk n-HXD, being in accord with the literature values of 291.3 K and 292.1 K [60,61], with its decrease from 5 K down to 24.5 K for the mean pore size of 300 Å and 60 Å down to $T_m(60\text{ Å}) = 266.8$ K for the maximal confinement. A similar decreasing trend is observed for the latter property from $\Delta H_m(\text{bulk}) = 222.4$ J/g n-HXD for the bulk n-HXD medium, being within 5.5% to the literature values of 236.3 J/g and 235.5 J/g n-HXD [60,61], down to $\Delta H_m(60\text{ Å}) = 124.5$ J/g n-HXD in the most confined n-HXD/SG 60 Å system. The extent of amorphization of the confined n-HXD increases from ca. 19% through ca. 36% up to 44% for the decreasing mean pore size from 300 Å through 100 Å down to 60 Å. The observed DSC findings mean that the confinement of n-HXD in SG matrices (1) accelerates the order-disorder change of its crystalline phase which occurs at lower T_m's and at the same time, (2) reduces order or increases disorder of the confined n-HXD sample due to its partial amorphization with respect to the original crystalline bulk state for $D_{\text{pore}} \to \infty$.

Our empirical trends of are fully consistent with and confirm those from several previous works on non-polar and polar organics [7–13] and can be further analyzed as follows. First, i.e., the change of melting temperature in the confined systems is often interpreted by means of the well-known Gibbs-Thompson (GT) equation [14]:

$$\begin{aligned}
T_m(D_{\text{pore}}) &= T_{m,\text{bulk}} - 2(\gamma_{\text{ws}} - \gamma_{\text{wl}}) \\
&\quad \times T_{m,\text{bulk}}/(D_{\text{pore}}\Delta H_{m,\text{bulk}}\rho_{\text{s}}) \\
&= T_{m,\text{bulk}} - K/D_{\text{pore}},
\end{aligned} \tag{1}$$

where $T_{m,\text{bulk}}$ and $T_m(D_{\text{pore}})$ are the melting temperatures of the bulk and the confined material, respectively, γ_{ws} and γ_{wl} are the corresponding wall-solid and wall-fluid

surface tensions, ρ_{s} is the density of the bulk liquid and $\Delta H_{m,\text{bulk}}$ is the latent heat of melting in the bulk state. Figure 5 presents a test of this standard thermodynamic model on n-HXD/SG systems. The decrease of $T_m(D_{\text{pore}})$ comparison to the bulk n-HXD suggests that the depression of melting of n-HXD with the reduction of pore size is connected with the $\gamma_{\text{ws}} > \gamma_{\text{wl}}$ relation which leads to the positive shift $\Delta T_m(D_{\text{pore}}) > 0$. In connection with the GT equation, molecular simulations on the simple non-polar Lennard-Jones molecular model (methane) confined in cylinder pores [62] revealed that the reduction in phase transition temperatures occurs when the mutual liquid-liquid interactions in the system are stronger than the liquid-wall ones. This appears to be further in accord with the empirical finding which follows from a combined DSC and infrared (IR) study on two non-polar media in silicagels (SG), namely, n-hexane and benzene [63]. Whereas in the latter case a specific (solvophilic) interaction between π-system of benzene and silanol groups of SG occurs, this is absent for non-polar n-alkane in the same SG matrix.

Second, i.e., the observed reduction of melting enthalpy in the confined systems in cylindrical pore can be interpreted by means of the Amanuel-Bauer-Bonventre-Lasher (ABBL) equation [64]:

$$\begin{aligned}
(\Delta H_m/\Delta H_{m,\text{bulk}})^{1/2} &= (\rho_{\text{part}}/\rho_{\text{total}})^{1/2}(1 - t/R_{\text{pore}}) \\
&= a - b/R_{\text{pore}},
\end{aligned} \tag{2}$$

which ascribes this change to the presence of nonfreezing interfacial layer in melting of crystallizing confined substance. Here, ΔH_m is the apparent enthalpy of melting of confined compound in J/g, $\Delta H_{m,\text{bulk}}$ is the bulk enthalpy of melting in J/g, m_{part} is the mass of compound participating in melting in g, m_{total} is the total mass of the confined compound in g, ρ_{part} is the density of compound
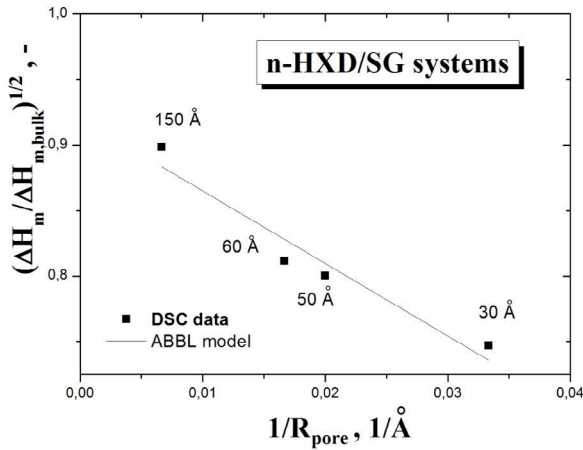
Fig. 6. Test of the Amanuel-Bauer-Bonventre-Lasher equation for the melting enthalpy in terms of $[\Delta H_m(R_{\mathrm{pore}})/\Delta H_{m,\mathrm{bulk}}]^{1/2}$ vs. $1/R_{\mathrm{pore}}$ plot.
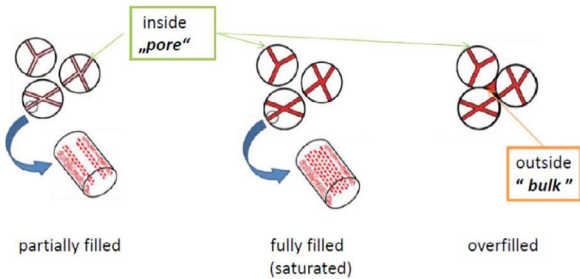
Fig. 7. Schematic models of the variously filled n-HXD/SG systems.

participating in melting, ρ_{total} is the average density of the confined compound, t is the thickness of the nonfreezing layer of the confined compound and R_{pore} is the pore radius. Application of this model provides the estimated value of interfacial thickness of nonfreezing n-HXD in SG matrices to be 9 ± 1 Å (Fig. 6).

All our DSC findings about phase separation in the n-HXD/SG systems are consistent with those found for the confined states of a bit longer n-alkanes: n-eicosane ($C_{20}H_{42}$) and n-heneicosane ($C_{21}H_{44}$) in the nanochannels of the MCM-41 matrix from a ^{13}C-NMR study [19]. The authors attributed the mobile amorphous phase of these confined n-alkanes to its localization in the interface region of the matrix pore due to the frustration in ordering of the relatively long chains in the vicinity of the surface wall of the matrix pore and the rigid or less mobile crystalline region in the central part, the so-called "core", of the matrix pore. This assignement is acceptable also for our case of n-HXD sample and appears to be strongly supported by the decreasing crystallinity in the partially filled n-HXD/SG samples as represented by the normalized melting enthalpy in Figure 2b. Figure 7 summarizes a schematical model of the changes in phase structure of n-HXD in the three differently filled n-HXD/SG systems proposed on the basis of the measured and analyzed DSC data by us and the literature NMR ones.
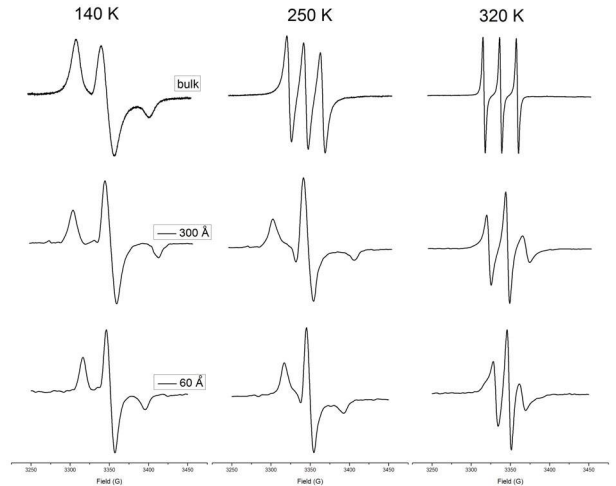

Fig. 8. Representative ESR spectra of the spin probe TEMPO in the bulk n-HXD, and in the restricted n-HXD/SG 300 Å and n-HXD/SG 60 Å systems at three selected temperatures: 140 K, 250 K and 320 K.

3.2 ESR responses and the characteristic ESR temperatures

Microscopic characterizations of bulk n-HXD and confined n-HXD/SG systems were carried out by measuring the dynamic behavior of the spin probe TEMPO by ESR. Figure 8 shows the representative ESR spectra of the spin probe TEMPO in the three spin systems at several selected temperatures in the whole measured T range from 100 K up to 320 K–350 K: in the bulk state of n-HXD (a) and in the two limiting confined saturated states of the n-HXD/SG with the largest (b) and smallest (c) pores of the D_{pore} value of 300 Å or 60 Å, respectively. The common feature of almost all of the ESR spectra is the characteristic triplet signal of the stable nitroxide radical due to interaction of the unpaired electron with the nitrogen atom of the nuclear spin number $I = 1$. The observed ESR spectra exhibit some further features common for all the investigated spin systems and other ones being distinct between bulk and confined systems. In both, the bulk and confined types of the spin systems, the respective ESR signal changes from a broad triplet in the low-T range to motionally narrow one at relatively higher temperatures. This most pronounced change of the spectral shape from a broad triplet to a motionally narrow one reflects a transition in the spin probe TEMPO dynamics from the slow motional regime to the fast one due to motional modulation (averaging) of the magnetic anisotropies, namely, the g and A tensors governed by a correlation time for the motion. On the other hand, the distinct feature in the ESR spectra consists in the linewidth variation, i.e., at the same temperatures the line width of the triplet signal increases with the decreasing the pore size.

Figure 9 displays a more detailed spectral evolution in the confined n-HXD/SG 100 Å system over a wide temperature range. Three regions of different spectral form can be distinguished: (1) a broad triplet in the low T range from 100 K up to 260 K followed by (2) intermediate
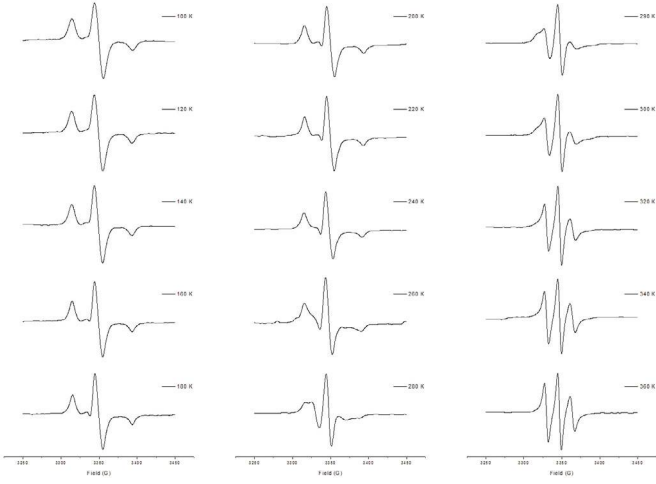
Fig. 9. Spectral evolution in the confined n-HXD/SG 100 Å systems with the mean pore diameter: $D_{\text{pore}} = 100$ Å over a wide temperature range from 100 K up to 360 K.

Fig. 10. Spectral parameter of mobility, $2A_{zz'}$ as a function of temperature for the bulk n-HXD and a series of the three confined n-HXD/SG samples. Colored vertical lines display the corresponding onset melting temperatures, $T_m(D_{\text{pore}})$ for the bulk ($D_{\text{pore}} \rightarrow \infty$) (black) and the three confined n-HXD/SG systems with $D_{\text{pore}} = 300$ Å (blue), 100 Å (green) and 60 Å (red).

region from ca. 270 K up to ca. 310 K, where superimposed triplets occur and finally, (3) a narrow triplet at higher temperatures above ca. 310 K. The remaining two confined systems with slightly changed boundary temperatures of the intermediate zone reveal similar spectral evolutions. This special aspect of the spin probe TEMPO dynamics in all the confined n-HXD/SG systems will be discussed in detail below.

Figure 10 displays the temperature dependence of the spectral parameter of mobility, $2A_{zz'}$, for the mean pore diameter, D_{pore}, as geometric parameter of the spin system in the bulk state ($D_{\text{pore}} = \infty$) and in the particular confined ones. Dramatic changes are evident in both the $2A_{zz'}(T)$ values with various degree of saturated confinement of the n-HXD media and their temperature dependencies. First, the $2A_{zz'}(T)$ values for the confined n-HXD samples are significantly higher over the entire investigated temperature range including both the slow and fast motional regimes in comparison with the corresponding values for the bulk n-HXD: $2A_{zz'}(T)$ (conf) $\gg 2A_{zz'}(T)$ (bulk). Furthermore, at the lowest temperature of our ESR measurements of 100 K in the slow motional regime, the $2A_{zz'}$ values for the saturated confined n-HXD/SG systems reach relatively high values of about 80 Gauss with the slightly lower $2A_{zz'}$ value for the larger pore size. On the other hand, in the bulk n-HXD this value is essentially lower and appears at level of 68 Gauss [55]. In the fast motional regime at higher temperatures above ca. 310 K, for three confined n-HXD/SG systems, the $2A_{zz'}$ parameter reaches the value of about 40 Gauss compared to the significantly lower $2A_{zz'}$ values in the bulk n-HXD medium. The most pronounced effect in the $2A_{zz'}$ vs. T plot is a transition of the spin probe TEMPO from the slow to fast motion regime at the conventionally defined characteristic ESR temperature $T_{50\,\text{G}}$. Whereas its value for the bulk n-HXD reaches a relatively low value of 192 K [55], for all the confined systems the respective $T_{50\,\text{G}}$'s are significantly higher, about
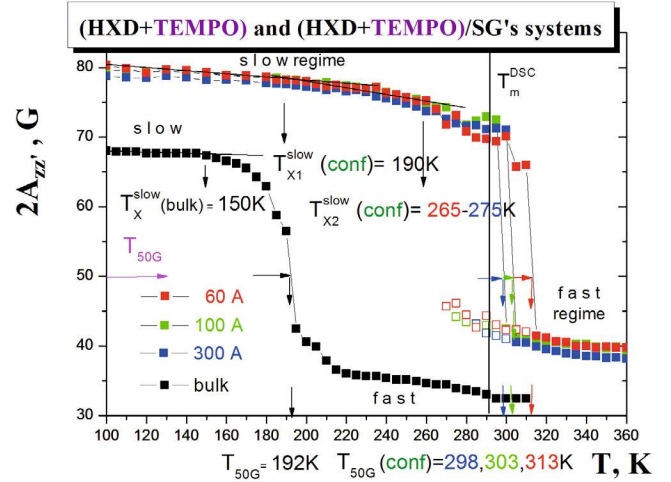
90–110 K: $T_{50\,\text{G}}$ (conf) $\gg T_{50\,\text{G}}$ (bulk) with a weakly increasing tendency with the decrease of mean pore diameter ranging from $T_{50\,\text{G}}(300$ Å$) = 298$ K through $T_{50\,\text{G}}(100$ Å$) = 303$ K up to $T_{50\,\text{G}}(60$ Å$) = 313$ K. All these findings indicate very strong slowing down effect of the confinement on the spin probe TEMPO reorientation in the (n-HXD + TEMPO)/SG systems compared to that in the bulk n-HXD/TEMPO one. The origin of this main effect of the spatial restriction on n-HXD embedded in SG matrices will be discussed later.

In addition to the main dynamic transition of the spin probe TEMPO at $T_{50\,\text{G}}$, some further characteristic features in the slow motional regime can be found. Thus, the slight decrease in the $2A_{zz'}$ occurs at the first characteristic ESR temperature, $T_{\text{X1}}^{\text{slow}}$(conf) which is situated at around 190 K in all the confined systems followed by the second one, $T_{\text{X2}}^{\text{slow}}$ (conf) ranging from 265 K up to 285 K, i.e., ca. 50–10 K below the respective slow to fast transition $T_{50\,\text{G}}$. This latter larger reduction in the $2A_{zz'}$ coincides with the observed appearance of the super-imposed triplet signals as seen in the spectral evolution of the representative n-HXD/SG 100 Å system (Figs. 9 and 10).

4 Discussion

All the observed ESR features indicate that the confinement of TEMPO dissolved in n-HXD in a series of SG matrices significantly alters the spin probe mobility compared to the bulk n-HXD. Thus, these ESR findings could serve as a microscopic indicator of the changed structural-dynamic state of the n-HXD/SG systems with respect to the bulk n-HXD. However, the situation is not simple because we face the basic question: what is the origin of the

spin probe TEMPO slowing down after confinement of its very dilute solution in n-HXD embedded in a series of SG matrices? The answer is complicated by the appearence of phase separation after confinement and the closely related localization aspect of the spin probe TEMPO, but the problem can be resolved by considering the relevant aspects: (i) the geometric factor, i.e., finite pore size effect of the used SG matrix and (ii) the mutual interaction factor between all the three components of the confined (n-HXD + TEMPO)/SG system as follows.

4.1 Phase separation and geometric effect of the spatial restriction on the phase structure and probe dynamics

As for the first aspect, from comparison of the characteristic ESR and DSC temperatures vs. $1/D_{\mathrm{pore}}$ plots motivated by equation (1) in Figure 5 quite different trends of the slow to fast transition and the phase transformation with confinement are evident. In particular, in contrast to the bulk n-HXD, for which $T_{50\,\mathrm{G}}$ (bulk) $\ll T_{m,\mathrm{bulk}}$ [55], all the three confined n-HXD/SG systems exhibit quite opposite relationship: $T_{50\,\mathrm{G}}$ (conf) $> T_m$ (conf) which means that all the spin probes TEMPO passed completely from the slow into the fast motion regime above the respective $T_m(D_{\mathrm{pore}})$, i.e., well in the liquid state of the confined n-HXD. Then, the spin probe TEMPO mobility above the corresponding $T_m(D_{\mathrm{pore}})$, but below the respective $T_{50\,\mathrm{G}}(D_{\mathrm{pore}})$ occurs in the "restricted" liquid state of n-HXD, while above both $T_m(D_{\mathrm{pore}})$ as well as $T_{50\,\mathrm{G}}(D_{\mathrm{pore}})$ in the "free" liquid one of n-HXD.

The opposite relationship between $T_{50\,\mathrm{G}}(D_{\mathrm{pore}})$ and $T_m(D_{\mathrm{pore}})$, i.e., $T_{50\,\mathrm{G}}$(bulk) $\ll T_{m,\mathrm{bulk}}$ and $T_{50\,\mathrm{G}}$(conf) $> T_m$(conf), and the observed anti-correlation trend between the $T_{50\,\mathrm{G}}$ and T_m vs. pore size D_{pore} plots indicate the quantitative and qualitative difference in the dynamic behavior of the spin probe TEMPO in the bulk n-HXD and the confined n-HXD/SG systems. In particular, we observe slowing down of the spin probe TEMPO rotation with increasing disorder of the confined n-HXD samples. This apparent paradox, i.e., spin probe TEMPO is more mobile in the crystalline n-HXD sample and less mobile in the significantly disordered n-HXD/SG systems suggests quite distinct mechanisms of the slow to fast transition dynamics in the crystalline bulk n-HXD sample and the partially crystalline n-HXD embedded in a series of SG matrices. In our previous paper about the spin probe TEMPO dynamics in bulk n-HXD, it was demonstrated by using the PALS data that the relationship $T_{50\,\mathrm{G}} \ll T_{m,\mathrm{bulk}}$ can be explained within the defect concept [55]. For the thermodynamic reason the spin probe TEMPO is preferentially trapped in the interlamellar gap of the crystalline lamellae of n-HXD and consequently, its slow to fast transition is connected with an deformation induced enhanced mobility of the end bonds of the chains in accord with the IR data about the higher conformational mobility of the end bonds in the pure n-alkanes. The present ESR and DSC findings $T_{50\,\mathrm{G}}$(bulk) $\ll T_{50\,\mathrm{G}}$ (300 Å) $< T_{50\,\mathrm{G}}$ (100 Å) $< T_{50\,\mathrm{G}}$ (60 Å) together with

this interpretation strongly suggests that the spin probes TEMPO are localized predominantly in the amorphous regions of the partially disordered n-HXD/SG system and not in the defect regions of the crystallites in the core of the confined samples. This morphological assignement is supported by the afore-mentioned ^{13}C-NMR study a bit longer n-alkanes $C_{20}H_{42}$ and $C_{21}H_{44}$ confined in the nanochannels of MCM-41 matrix [19]. However, in addition to this first possibility of the spin probe TEMPO localization in the amorphous interface region in consistency with its thickness, other part of the spin probes can be localized in the disordered domains situated also in the "core" region in between the n-HXD crystals.

Moreover, in the case of the saturated confined n-HXD/SG systems, a detailed inspection of the spectral evolution of the ESR signals, as demonstrated for the n-HXD/SG 100 Å system in Figure 9 (and similarly for the remaining two fully filled confined samples – not shown) and the related temperature dependence of the spectral parameter of mobility, $2A_{zz'}$, in Figure 10, reveals the presence of two kinds of the differently moving spin probes TEMPO giving both broad and narrow triplets. This coexistence of two distinct populations of TEMPO indicates the dynamic heterogeneity of spin probe TEMPO in the complex confined system and reflects their different local structural-dynamic microenvironments. A part of the spin probes TEMPO moves rapidly just after melting of the n-HXD filler and the other one remains still relatively immobilized up to about 10 K–40 K above the respective $T_m(D_{\mathrm{pore}})$. Tentatively, the slowly moving one above the corresponding $T_m(D_{\mathrm{pore}})$ can be ascribed to the fraction of the spin probes localized at the amorphous interface region of the SG pores in accord with an estimation of its thickness (spin probe TEMPO size given by its equivalent van der Waals radius is $R_W^{\mathrm{eq}} = 3.45$ Å). On the other hand, the fast moving part of the spin probes in sub-$T_{50\,\mathrm{G}}$ region may be ascribed to the TEMPO molecules localized in this amorphous interphase being mobilized by melting as well as in the amorphous phase in between the crystals in the central "core" region of the pore. On further increase the temperature above the corresponding $T_m(D_{\mathrm{pore}})$, all the spin probes TEMPO become moving in the fast motion regime with still significantly slower mobility compared to the spatially unrestricted bulk n-HXD.

To address this special free radical probe localization aspect of the confinement problem we have performed ESR measurements with a series of the n-HXD/SG 100 Å systems filled to various extent. Figure 11 displays the $2A_{zz'}$ vs. T plots for the following three cases, namely, the partially filled sample with $F_{HXD} = 0.1564$, the completely filled (saturated) one with $F_{HXD,sat} = 0.325$ and finally, the overfilled case with $F_{HXD} = 0.55$. The $2A_{zz'}(T)$ values over the entire temperature range and $T_{50\,\mathrm{G}}$ for the first partially filled situation reach the highest values. These findings together with the included $T_m(D_{\mathrm{pore}} = 100$ Å, $F_{\mathrm{HXD}} = 0.1564)$ line indicate that the spin probes TEMPO seem to be localized in the amorphous surface layer of pore due to the preferential wetting the pore surface by the n-HXD liquid. This appears to
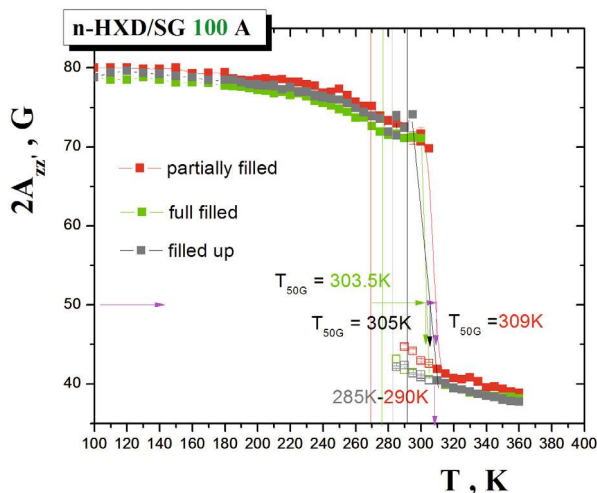
Fig. 11. Spectral parameter of mobility, $2A_{zz'}$ as a function of temperature for a series of the three confined n-HXD/SG 100 Å samples with various extent of filling: partially filled with $F_{HXD} = 0.1564$ (red), fully filled with $F_{HXD} = 0.325$ (green) and overfilled with $F_{HXD} = 0.55$ (gray). Color vertical lines display the corresponding onset melting temperatures, $T_m(D_{pore} = 100$ Å, $F_{HXD} = 0.1564$ (red), 0.325 (green) and 0.55 (gray)) as well as for the bulk state T_m ($D_{pore} \to \infty$) (black).

be consistent with the largest difference between the occurency of the fast component at 290 K and $T_m(D_{pore} = 100$ Å, $F_{HXD} = 0.1564) = 269$ K. On the other hand, the $2A_{zz'}(T)$ and $T_{50\,G}$'s for the remaining two confined samples are a bit lower and rather close to each other suggesting a partial contribution from localization of the spin probes TEMPO in the amorphous phase between the n-HXD crystals inside the pores in the full filled sample and in both inside as well as outside the pores in the overfilled system.

4.2 The mutual interaction effects between the components of the confined systems

The previous paragraph suggests that the spin probes TEMPO are situated in the amorphous regions of the saturated partially crystalline confined n-HXD/SG systems and that they can be localized at the surface of the interface region of the pore and in the amorphous phase between the n-HXD crystals in the core region of the pore. In further discussion of the preferential type of the spin probe localization in these amorphous regions of the confined n-HXD, we have to keep in mind that two basic types of the intermolecular interactions of the spin probe TEMPO exist in the investigated three-component confined systems, i.e., that between the polar TEMPO and the non-polar n-HXD molecules and that between the polar TEMPO and the polar SG matrix. Then, concerning the second possible origin of the spin probe TEMPO deceleration, our attention is focused on the spectral parameter of mobility, $2A_{zz'}$, for the spin probe TEMPO in both the bulk and confined liquid states. In this context it is useful

to compare their values of about 33 and 40 Gauss in both the bulk n-HXD and the confined n-HXD/SG system with some typical ones of nitroxyl free radicals in various types of non-polar and polar media (solvents or substrates) as well as for similar combined systems as obtained from other ESR experiments and from theoretical calculations. It is well-known that the typical value of $2A_{zz'}$ for nitroxyl free radicals in a typical non-polar liquid such as toluene achieves the value of about 34 Gauss, while in hydrogen bonded organics such as phenol the value is about 38 Gauss – see, e.g. [65]. The former value is fully consistent with the fast moving spin probe TEMPO in the non-polar bulk liquid n-HXD. This is in contrast to the latter being close to the fast regime in the confined states of n-HXD in the SG matrices. Further, the higher $2A_{zz'}$ value of the TEMPO in the fast regime in the confined state of the SG matrices reaching about 40 Gauss is comparable with the reported one of 39 Gauss for the similar spin probe di-terc-butyl nitroxide (DTBN) adsorbed in silica gel at RT [65]. This significantly enhanced value suggests some specific interactions between the TEMPO molecule and the silanol Si-O-H group at the surface wall of the pore of the SG matrices.

In addition to these empirical arguments, this hypothesis can be supported by the reported quantum-mechanical calculations of the $2A_{zz'}$ quantity for the free DTBN radical modelling its presence in non-interacting non-polar medium and for the simplest H-O-H + DTBN spin system approximately simulating the silanol group and nitroxyl free radical interaction [66]. The former case provided the value of 33 Gauss, while in the latter one the essentially higher value of 38 Gauss was found. The latter calculations were performed with the aim to explain similar dramatic increase of $2A_{zz'}$ parameter of nitroxyl spin probe in a composite system of poly(ethylene) with SG [66]. Our case of confined n-HXD/SG systems can be considered as a just reverse situation of non-polar medium in the pores of SG indicating the essential role of intermolecular interaction of the radical fragment $\bullet$O-N< from the free radical probe with the H-atoms of silanol groups in the inner surface wall in the partially and full filled n-HXD/SG samples and also with the external surface wall of the SG matrix in the overfilled one. All these empirical and theoretical findings strongly support the hypothesis about free TEMPO in non-polar van der Waals n-HXD and about the significantly immobilized TEMPO at the polar surface of SG matrix filled with the non-polar n-HXD medium. Consequently, due to this specific interaction of molecular probe TEMPO with the SG matrix this spin probe does not correctly reflect the changed structural-dynamics in the confined non-polar n-HXD medium in this SG matrix. It is of natural interest to investigate other types of filler with larger affinity to the surface of matrix. Work in this direction is in progress.

5 Conclusions

We presented the results of a joint microscopic ESR and macroscopic DSC study of the change of the

guest molecule dynamics and the phase behavior in n-hexadecane (n-HXD) confined in a series of silica gel (SG) matrices. In contrast to the bulk n-HXD, where the spin probe TEMPO dynamics is controlled by the local interlamellar gap defect properties, the combined ESR and DSC study indicates that the spin probe mobility in the various partially filled, full filled as well as the over-filled confined states of the very dilute solution of polar TEMPO in the non-polar n-HXD solvent embedded in the polar SG matrices is governed mainly by its specific interactions with surface walls of the SG matrix. This points to the significant role of the mutual relative interactions between all three components in any external probing of organic compound confined in inorganic host and the limited validity for characterization of the changed structural-dynamic state of non-polar medium due to its geometrical confinement in polar matrix via polar molecular probe.

References

1. C. Alba-Simionesco, B. Coasne, G. Dosseh, G. Dudziak, K.E. Gubbins, R. Radhakrishnan, M. Sliwinska-Bartkowiak, J. Phys.: Condens. Matter **18**, R15 (2006)
2. M. Alcoutlabi, G.B. McKenna, J. Phys.: Condens. Matter **17**, R461 (2005)
3. M. Koza, B. Frick, R. Zorn (Eds), Eur. Phys. J. Special Topics **189** (2010)
4. M. Koza, B. Frick, R. Zorn (Eds), Eur. Phys. J. Special Topics **141** (2007)
5. M. Koza, B. Frick, R. Zorn (Eds), Eur. Phys. J. E **12** (2003)
6. B. Frick, R. Zorn, H. Büttner (Eds), J. Phys. IV **10** (2000)
7. C.L. Jackson, G.B. McKenna, J. Chem. Phys. **93**, 9002 (1990)
8. R. Mu, V.M. Malhotra, Phys. Rev. B **44**, 4296 (1991)
9. K.M. Unruh, T.E. Huber, C.A. Huber, Phys. Rev. B **48**, 9021 (1993)
10. M. Sliwinska-Bartkowiak, J. Gras, R. Sikorski, R. Radhakrishnan, L. Gelb, K.E. Gubbins, Langmuir **15**, 6060 (1999)
11. M.R. Landry, Thermochim. Acta **433**, 27 (2005)
12. M. Baba, J.D. Nedelec, J. Lacoste, J.L. Gardette, M. Morel, Degr. Polym. Stab. **80**, 305 (2003)
13. N. Bahloul, M. Baba, J.M. Nedelec, J. Phys. Chem. B **109**, 16227 (2005)
14. R. Evans, U.M.B. Marconi, J. Chem. Phys. **86**, 7138 (1987)
15. C. Alba-Simionesco, G. Dosseh, E. Dumont, B. Frick, B. Geil, D. Morineau, V. Teboul, Y. Xia, Eur. Phys. J. E **12**, 19 (2003)
16. P. Huber, D. Wallacher, J. Alberts, K. Knorr, Eur. Phys. Lett. **65**, 35 (2004)
17. P. Huber, V.P. Soprunyuk, K. Knorr, Phys. Rev. E **74**, 031610 (2006)
18. A.E.W. Hansen, F. Courivaud, A. Karlsson, S. Kolboe, M. Stocker, Micropor. Mesopor. Mater. **22**, 309 (1998)
19. M. Okazaki, K. Toriyama, S. Anandan, Chem. Phys. Lett. **401**, 363 (2005)
20. A.F. Kremer, A. Huwe, A. Schönhals, A.S. Rozanski, in *Broadband Dielectric Spectroscopy*, edited by F. Kremer, A. Schönhals (Springer-Verlag, Berlin, 2002), p. 171
21. M. Sliwinska-Bartkowiak, G. Dudziak, R. Sikorski, N. Gras, R. Radhakrishnan, K.E. Gubbins, J. Chem. Phys. **114**, 950 (2001)
22. A. Huwe, M. Arndt, F. Kremer, C. Haggenmueller, P. Behrens, J. Chem. Phys. **107**, 9699 (1997)
23. P. Pissis, D. Daoukaki-Diamanti, L. Apekis, C. Christodoulides, J. Phys.: Condens. Matter **6**, L325 (1994)
24. R. Zorn, D. Richter, L. Hartmann, F. Kremer, B. Frick, J. Phys. (France) **10**, 7 (2000)
25. R. Zorn, B. Frick, L. Hartmann, F. Kremer, A. Schönhals, D. Richter, Physica B **350**, e1115 (2004)
26. J. Baumert, B. Asmussen, C. Gutt, R. Kahn, J. Chem. Phys. **116**, 10869 (2002)
27. T. Hofmann, D. Wallacher, M. Mayorova, R. Zorn, B. Frick, P. Huber, J. Chem. Phys. **136**, 124505 (2012)
28. *Molecular Dynamics in Restricted Geometries*, edited by J.M. Drake, J. Klafter (Wiley and Sons, New York, 1989)
29. J.M. Drake, J. Klafter, Phys. Today **43**, 46 (1990)
30. D. Dutta, P.K. Pujari, K. Sudarshan, S.K. Sharma, J. Phys. Chem. C **112**, 19055 (2008)
31. R. Zaleski, J. Goworek, Mat. Sci. Forum **607**, 180 (2009)
32. M. Iskrová, V. Majerník, E. Illeková, O. Šauša, D. Berek, J. Krištiak, Mat. Sci. Forum **607**, 235 (2009)
33. G.G. Cameron, in *Comprehensive Polymer Science*, edited by C. Booth, C. Price (Pergamon Press, Oxford, 1989), Vol. 1, p. 517
34. Z. Veksli, M. Andreis, B. Rakvin, Prog. Polym. Sci. **25**, 949 (2000)
35. D. Banerjee, S.N. Bhat, S.V. Bhat, D. Leporini, Proc. Natl. Acad. Sci. **106**, 11448 (2009)
36. D. Banerjee, S.N. Bhat, S.V. Bhat, D. Leporini, PLoS One **7**, e44382 (2012)
37. D. Banerjee, S.V. Bhat, D. Leporini, Adv. Chem. Phys. **152**, 1 (2013)
38. D. Leporini, X.X. Zhu, M. Krause, G. Jeschke, H.W. Spiess, Macromolecules **35**, 3977 (2002)
39. H. Yoshioka, J. Chem. Phys. Soc. Faraday Trans. I **84**, 4509 (1988)
40. G. Martini, M.F. Ottaviani, M. Romanelli, L. Kevan, Coll. Surf. **41**, 149 (1989)
41. G. Martini, Coll. Surf. **45**, 83 (1990)
42. S. Anandan, M. Okazaki, Micropor. Mesopor. Mater. **87**, 77 (2005)
43. G. Martini, M.F. Ottaviani, M. Romanelli, J. Coll. Interface Sci. **94**, 105 (1983)
44. M. Romanelli, M.F. Ottaviani, G. Martini, J. Coll. Interface Sci. **96**, 373 (1983)
45. G. Martini, Coll. Surf. **11**, 409 (1984)
46. G. Martini, M.F. Ottaviani, M. Romanelli, J. Coll. Interf. Sci. **115**, 87 (1987)
47. F. Mazzoleni, M.F. Ottaviani, G. Martini, J. Phys. Chem. **92**, 953 (1988)

48. M. Romanelli, M.F. Ottaviani, G. Martini, L. Kevan, J. Phys. Chem. **93**, 317 (1989)
49. M. Okazaki, K. Toriyama, K. Sawaguchi, K. Oda, Appl. Magn. Res. **23,** 433 (2003)
50. M. Okazaki, K. Toriyama, J. Phys. Chem. B **107**, 7654 (2003)
51. M. Okazaki, K. Toriyama, K. Sawaguchi, K. Oda, Bull. Chem. Soc. Jpn **77**, 87 (2004)
52. M. Okazaki, K. Toriyama, J. Phys. Chem. B **109**, 13180 (2005)
53. M. Okazaki, K. Toriyama, J. Phys. Chem. B **109**, 20068 (2005)
54. M. Okazaki, S. Anandan, S. Seelan, M. Nishida, K. Toriyama, Langmuir **23**, 1215 (2007)
55. J. Bartoš, H. Švajdlenková, M. Zaleski, M. Edelmann, M. Lukešová, Physica B **430**, 99 (2013)
56. G.P. Rabold, J. Polym. Sci. A **17**, 121 (1969)
57. J. Bartoš, H. Švajdlenková, G. Dlubek, Y. Yu, R. Krause-Rehberg, Chem. Phys. Lett. **584**, 88 (2013)
58. H. Švajdlenková, O. Šauša, M. Iskrová-Miklošovièová, V. Majernik, J. Krištiak, J. Bartoš, Chem. Phys. Lett. **539**, 39 (2012)
59. H. Švajdlenková, J. Bartoš, J. Polym. Sci. B **47**, 1058 (2009)
60. M.G. Broadhurst, J. Res. Natl. Bur. Stand. **66A**, 241 (1962)
61. M. Dirand, M. Bouroukba, V. Chevallier, D. Petitjean, J. Chem. Eng. Data **47**, 115 (2002)
62. M.W. Maddox, K.E. Gubbins, J. Chem. Phys. **107**, 9659 (1997)
63. T. Takei, T. Konishi, M. Fuji, T. Watanabe, M. Chikazawa, Thermochim. Acta **267**, 159 (1995)
64. S. Amanuel, H. Bauer, P. Bonventre, D. Lasher, J. Phys. Chem. C **113**, 18983 (2009)
65. G.P. Lozos, B.M. Hoffman, J. Phys. Chem. **78**, 2110 (1974)
66. J. Tiňo, P. Mach, Z. Hloušková, I. Chodák, J. Macromol. Chem. Pure Appl. Chem. A **31**, 1481 (1994)